# An Intense $\gamma$-ray Beam Line of 10 MeV Order Based on Compton Backscattering

W. Guo [a,b,*], W. Xu [a], J.G. Chen [a], Y.G. Ma [a], X.Z. Cai [a], H.W. Wang [a], Y. Xu [a,b], C.B. Wang [a,b], G.C. Lu [a], R.Y. Yuan [a], J.Q. Xu [a], Z.Y. Wei [a], Z. Yan [a], W.Q. Shen [a]

[a] *Shanghai Institute of Applied Physics, Chinese Academy of Sciences, Shanghai 201800, China*

[b] *Graduate School of the Chinese Academy of Sciences, Beijing 100039, China*

**Abstract**

Shanghai Laser Electron Gamma Source, a $\gamma$-ray beam line of 10MeV order was proposed recently. The beam line is expected to generate $\gamma$-ray with maximum energy of 22MeV by backward Compton scattering between $CO_2$ laser and electron in the 3.5GeV storage ring of future Shanghai Synchrotron Radiation Facility. The flux of non-collimated $\gamma$-ray can be $10^9 \sim 10^{10}$ $s^{-1}$ if a commercial $CO_2$ laser of 100W order output power is employed and injected with optimized settings.

*Key words:* Compton backscattering, Gamma ray source,
*PACS:* 13.60.Fz, 41.75.Ht, 07.85.Fv

## 1. Introduction

Compton backscattering (CBS) of laser light against relativistic electron could be a promising method to obtain polarized monochromatic $\gamma$ rays with small divergence angle. This idea was pointed out by Milburn (1), Arutyunian and Tumanian (2) for the first time in 1963.

Among $\gamma$-ray producing techniques, CBS method possesses several significant advantages (3). First, Compton scattering is well understood within QED framework, and there are definite relations among energy, emitting angle, cross section, polarization, etc. of the scattered photons. Second, the scattered photons has a sharp cut-off near the maximum energy and the largest fraction of photons is in the high energy region. Third, CBS $\gamma$-rays based on relativistic $e^-$ have a very small divergence angle, that allows experiments with both compact targets and detectors. Fourth, CBS method provides a convenient and swift way to steer the polarization of $\gamma$-rays by changing polarization of injected laser beams.

The first $\gamma$-ray facility based on CBS method, the LADON beam, started to operate in 1978 (4; 5; 6; 7). Till now, there are several $\gamma$-ray facilities all over the world (8). Most of them produce $\gamma$-ray from several hundred MeV to several GeV. Also, there are a few MeV $\gamma$-ray facilities: HI$\gamma$S(9; 10) on Duke storage ring, BL05SS(11; 12) on SPring-8 storage ring and BL-1(13; 14) on NewSUBARU.

The future Shanghai Synchrotron Radiation Facility (SSRF) (15) provides precious opportunity to build a $\gamma$ source of high quality. Recently, Shanghai Laser Electron Gamma Source (SLEGS), a $\gamma$-ray beam line based on CBS method has been proposed. In the coming sections, basic relations of CBS method will be described briefly, the proposed SLEGS facility and $\gamma$-ray it generated will be illustrated and compared with other CBS $\gamma$-ray

* Corresponding author.
*Email address:* guowei@sinap.ac.cn (W. Guo).

facilities of ten MeV order.

## 2. Basic Relations

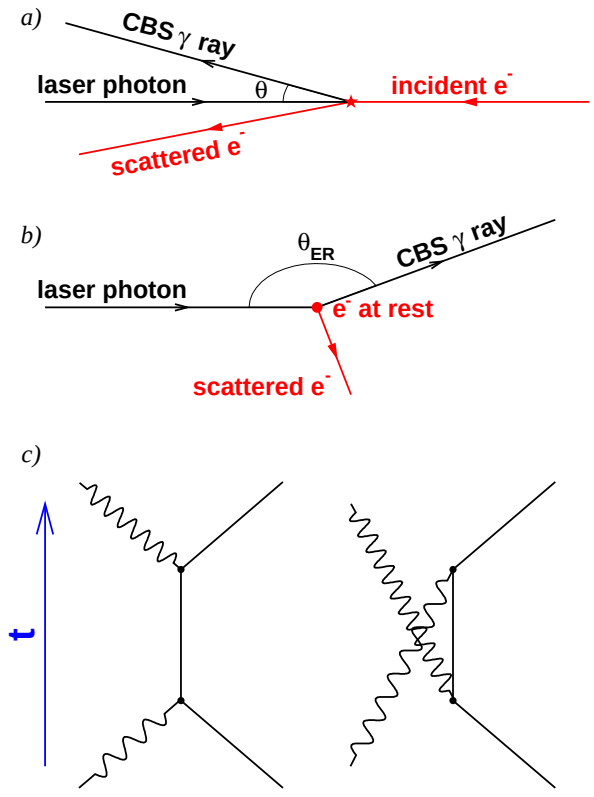


Fig. 1. Kinematics of CBS process between electron and laser photon in a) laboratory frame, b) electron rest frame, and c) Feynman diagram of Compton scattering.

Compton scattering between $e^-$ and photon can be described within QED framework(16). The kinematics of CBS in laboratory (LAB) frame a), electron rest (ER) frame b), and related Feynman diagram c) is shown as Fig.1.

Energy of CBS $\gamma$ photon $E_\gamma$ is related to the emitting angle $\theta$:

$$E_\gamma = \frac{(1+\beta)E_L}{1-\beta\cos\theta+(1+\cos\theta)E_L/E_0} \tag{1}$$

where $E_0$ is the energy of incident $e^-$, $\gamma = E_0/m_0c^2 = 1/\sqrt{1-\beta^2}$ the relativistic factor, $m_0c^2 = 0.511$ MeV mass of $e^-$ at rest and $E_L$ the energy of incident laser photon. In case of relativistic $e^-$, i.e., $\gamma \gg 1$ and $\beta \approx 1$, formula(1) can be simplified as:

$$E_\gamma = \frac{4\gamma^2 E_L}{1+4\gamma^2 E_L/E_0+\gamma^2\theta^2} \tag{2}$$

which indicates that the maximum energy of CBS photon is proportional to $\gamma^2$ approximately.

The angular differential cross-section of CBS $\gamma$-rays in ER frame follows Klein-Nishina formula(17). The angular differential cross-section in LAB frame can be derived by Lorentz transformation. In case of relativistic $e^-$, the angular divergence of CBS $\gamma$-rays in LAB frame is in order of $1/\gamma$.

When injected laser beam is totally polarized, the degree of polarization of CBS $\gamma$ photons has a clear relationship with the scattering angle(8).

The ideal flux $n_\gamma$ of CBS $\gamma$ rays is related to the impact geometry and spatial densities of electron and laser beams. The spatial density of electrons is treated as product of Gaussian distributions, the corresponding widths are determined by beam qualities and TWISS functions of the storage ring(18; 19; 20). The spatial density of laser is also treated as product of Gaussian distributions, the corresponding widths are determined by optics of Gaussian beams(21).

In a typical head-on setup, the ideal flux of CBS $\gamma$ rays is:

$$n_\gamma = P_0 I L \tag{3}$$

where $P_0$ is the laser power, $I$ the current of $e^-$ beam, and $L$ the luminosity:

$$L = \frac{2\sigma(1+\beta)}{\pi ceE_L}\int \frac{ds}{(4\sigma_x^2+w^2)^{\frac{1}{2}}(4\sigma_y^2+w^2)^{\frac{1}{2}}} \tag{4}$$

where $\sigma$ denotes the total Compton cross section, $w$ the transversal dimension of laser, $\sigma_{x,y}$ the horizontal and vertical width of the $e^-$ bunch respectively.

One should notice that the actual luminosity $L^*$ is significantly affected by geometrical restriction of both injected laser beam and extracted $\gamma$ beam, this is limited by vacuum tube dimensions of the storage ring. Henceforth, we applied proper selection on ideal CBS events during the Mote-Carlo simulation.

## 3. SLEGS Facility

A schematic view of future SLEGS facility is illustrated as Fig.2. Laser beam of operating wavelength is generated and polarized in the optical chamber,

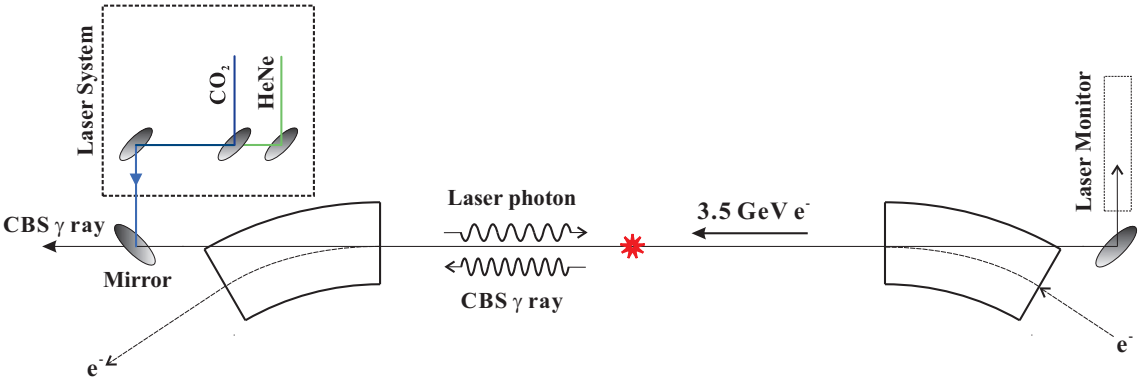


Fig. 2. A schematic view of future SLEGS facility.

then focused and injected into SSRF storage ring from front-end downstream to the selected sector, i.e., the interaction region by a thin mirror. The operating laser is aligned to the electron beam by a co-axis visible laser. Once laser beam overlaps $e^-$ bunches, Compton backscattering occurs between relativistic electron and laser photon, $\gamma$-ray with determined energy and a narrow divergence angle is generated, transported and then extracted from the inject front-end. After the rear-end upstream to the interaction region, remaining laser light is inspected by a set of monitors which provides feedback and control signals as well.

### 3.1. *SSRF and its storage ring*

SSRF, now under construction, will operate by year 2009. It will be a high performance third-generation synchrotron facility producing high brightness X-ray covering an energy range from 0.1keV to 40keV(15). It consists of an 100MeV LINAC, an 100MeV to 3.5GeV booster, a 3.5GeV storage ring and associated experimental stations. The storage ring has 4 identical long straight sectors, 16 identical standard straight sectors, and 40 bending magnets(22). Its designed features are listed in Table.1.

The future SLEGS facility can be constructed on one of the standard straight sectors of SSRF, probably on sector 20. TWISS functions of sector 20 is shown as Fig.3.

There are two kinds of vacuum tube assembled along SSRF storage ring. Vacuum tube for the bending sectors has a $\pm$7.5 mm vertical water-cooling slit to encapsulated microwave radiation of the RF, shown as Fig.4 . Such slits are the most confining parts for laser beam in transversal directions, hence-

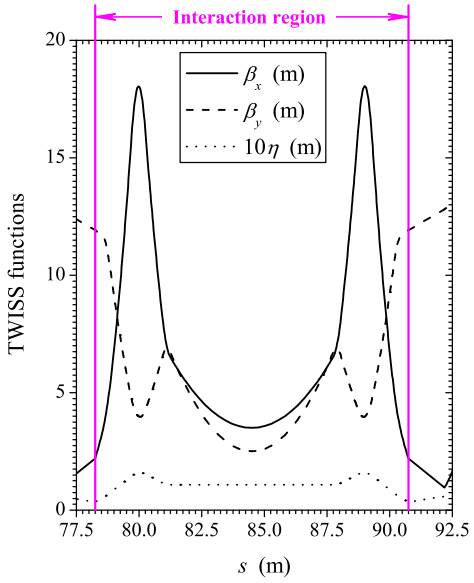


Fig. 3. TWISS functions of SSRF sector 20, calculated by MAD-9. Straight sector between bending magnets, i.e., the interaction region, is marked by a pair of vertical lines.

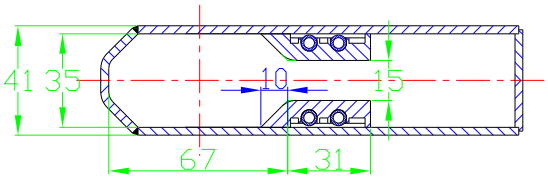


Fig. 4. Sectional dimensions of SSRF vacuum tube for bending sectors. The dash-dot lines denote the center orbit of electron bunches. The operating laser beam will be transported through the slit for outside(right) to inside(left).

Table 1
Designed features of SSRF storage ring.

| | | | |
|---|---|---|---|
| perimeter | | 432 | m |
| length of long straight | | 12.0 | m |
| length of standard straight | | 6.7 | m |
| radio frequency | | 499.65 | MHz |
| designed energy | $E_0$ | 3.5 | GeV |
| momentum dispersion | $\sigma_p$ | 0.1 | % |
| momentum acceptance | | 3.0 | % |
| transversal emittance | $\varepsilon_0$ | 3.9 | nm·rad |
| coupling factor | $\kappa$ | 1.0 | % |
| natural beam length | $\sigma_s$ | 4.0 | mm |
| beam current of single bunch mode | $I$ | 5.0 | mA |
| beam current of multi bunch mode | $I$ | 300 | mA |
| beam lifetime | | >10 | hrs |

forth cause a considerable limitation on the population of injecting photons, and consequentially limit the total flux of CBS $\gamma$-ray most.

### 3.2. *$CO_2$ Laser and Corresponding CBS $\gamma$-ray*

The fundamental wavelength of $CO_2$ laser is 10.64$\mu$m, the corresponding $E_L$ is 0.117eV. The maximum energy of CBS $\gamma$-ray of $CO_2$ laser with 3.5GeV electron is about 22MeV. Commercial $CO_2$ laser is widely used in many industrial fields. It has several advantages compared to molecular gas lasers with longer wave lengthes:

– well developed, compact, and with high qualities;
– high output power that promises a high flux of CBS $\gamma$-ray;
– run under both continuous and pulsed mode;
– relatively low cost and low technological risk;
– easy to manage and control.

The angular differential cross section and energies of CBS $\gamma$-ray from $CO_2$ laser against 3.5GeV electron is shown as Fig.5. Since maximum energy of BCS $\gamma$-ray ($\sim$22 MeV) is within the momentum acceptance of SSRF storage ring($\pm$105 MeV), all scattered electrons will be re-accelerated. Hence SLEGS can operate parasitically, independent of other users on SSRF in principle.

### 3.3. *Luminosity of CBS $\gamma$-ray*

The transversal restriction of SLEGS vacuum tube to the $CO_2$ laser beam is illustrated as Fig.6.

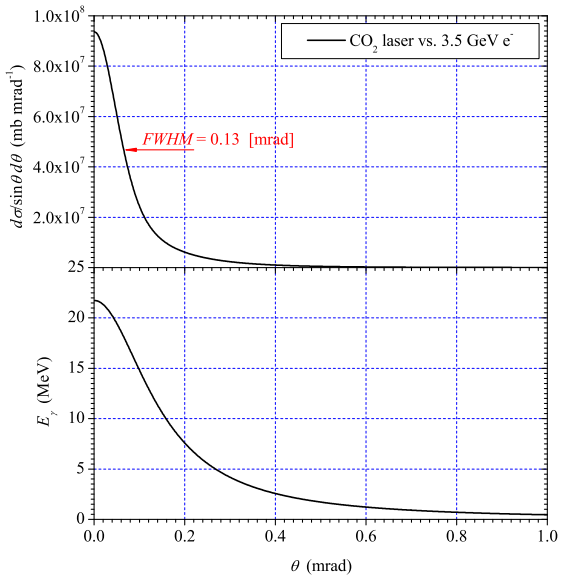


Fig. 5. The angular differential cross section (upper panel) and energies as a function of emitting angle $\theta$ (lower panel) of CBS $\gamma$-ray from $CO_2$ laser against 3.5GeV electron.

As we have mentioned above, slit of the bending magnet is the most confining position for injected $CO_2$ laser.

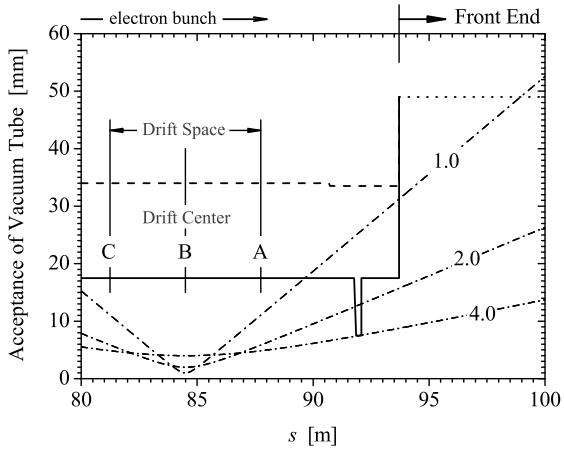


Fig. 6. Transversal restriction of SLEGS vacuum tube. The solid(dash) line represents the horizontal(vertical) boundary. Vacuum tube of the front end of SLEGS beam line is not finally determined yet, marked as a dotted line. The dash-dot lines represents transversal dimension $w$ of $CO_2$ laser focusing on the drift center with different waist widths $w_0 = 1.0, 2.0$ and 4.0 mm respectively. Direction of electron bunch is shown at the top.

We have developed a C++ program based on Monte-Carlo method to simulate the generation

of CBS $\gamma$-ray. First, configuration of SLEGS, laser/electron bunch parameters and TWISS functions are loaded; then, the related ideal luminosity with infinite acceptance is calculated. Second, the program starts to sample space coordinates of ideal CBS events according to the ideal luminosity distribution. Third, the program samples momentum coordinates for each incident laser photon, and checks if it can pass the geometrical restriction or not. Fourth, the scattered angles of CBS $\gamma$-ray are sampled according to differential cross section of Compton scattering. Last, the program checks if the CBS $\gamma$ ray is "actual", i.e., the $\gamma$ ray can pass the geometrical restriction or not.

In a head-on setup, flux of CBS $\gamma$ rays is related to the focusing position and waist dimension of laser beam, shown as Fig.7. Since the designing of SLEGS

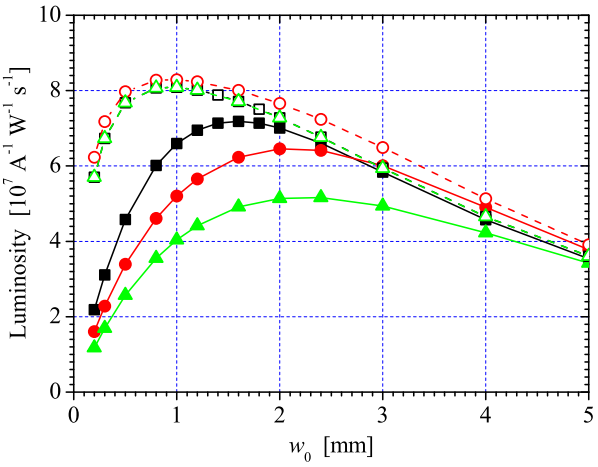


Fig. 7. Luminosity of CBS $\gamma$ rays in a head-on setup of $CO_2$ laser against SLEGS electron beam in multi bunch mode. See the text for explanations.

front end is now undergoing, we consider the flange connecting storage ring and front end as the inspecting plane. The laser power on the inspecting plane is considered to be the injected power, and CBS $\gamma$ rays that reach the inspecting plane are considered to be actual. We tried three different focuses for $CO_2$ laser: at the down-stream end (A), center (B) and up-stream end (C) of the drift space respecting to the beam direction of electron bunch, as shown in Fig.6. In Fig.7, solid and open symbols represent actual($L^*$) and ideal($L$) values respectively; squares, circles and triangles represent luminosity of different laser focusing position at A, B and C respectively. As we can see in Fig.7, although lasers with waist dimension of $\sim$ 1mm correspond to maximum $L$, the related values of $L^*$ are evidently limited by geometrical restriction.

The most optimized waist dimension for $CO_2$ laser is around 1.6mm, while the focus is on the down-stream side. In that case, we can obtain a maximum $L^* \sim 7 \times 10^7$ A$^{-1}$W$^{-1}$s$^{-1}$. Considering SSRF storage ring running under multi bunch mode($I_m = 300$ mA), the flux of BCS $\gamma$-ray is expected to be $\sim 10^{10}$ s$^{-1}$ if a CW $CO_2$ laser of 500 W is employed.

The estimated flux of CBS $\gamma$-ray per unit laser power gathered within a given collimation angle $\Theta$ is illustrated as Fig.8. The energy spectrum of CBS

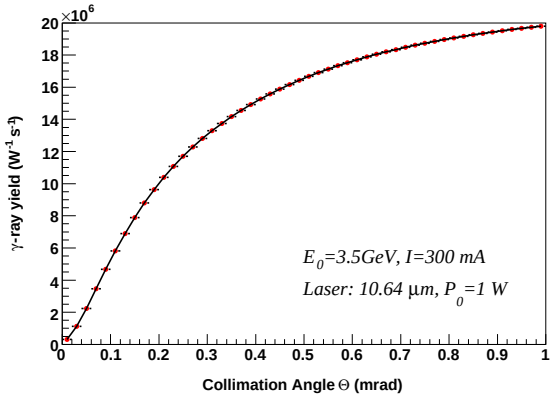


Fig. 8. Estimated flux of CBS $\gamma$ rays as a function of collimation angle.

$\gamma$-ray of different collimation angle is illustrated as Fig.9.

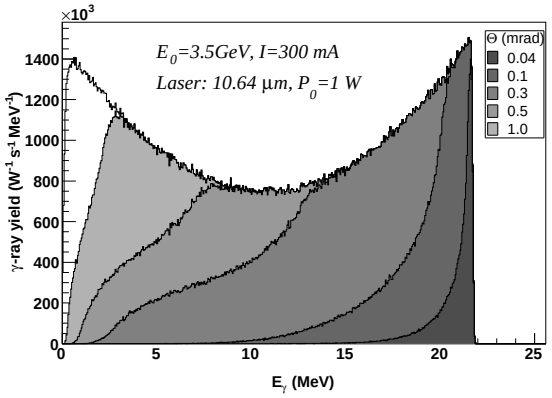


Fig. 9. The energy spectrum of CBS $\gamma$-ray of different collimation angle. The histograms filled with gray scale stand for collimation angle $\Theta$ of 0.04, 0.1, 0.3, 0.5 and 1.0mrad respectively. The histogram filled with white represents the non-collimated energy spectrum.

Table 2
CBS $\gamma$-ray facilities of 10 MeV order.

| facility | laser type | $\lambda$ ($\mu$m) | $P_0$ (W) | $E_\gamma^{\max}$ (MeV) | $\gamma$-ray flux ($s^{-1}$) |
|---|---|---|---|---|---|
| HI$\gamma$S on Duke storage ring(9) | free electron laser | | | 2∼58 | $5 \times 10^7$ |
| BL05SS on SPring-8(11) | $CO_2$ pumped $CH_3OH$ laser | 119 | 2 | 10 | $10^5$ |
| BL-1 on NewSUBARU(13) | Nd:$YVO_4$ laser | 1.064 | 0.74 | 17.6 | $1.3 \times 10^7$ |
| SLEGS on SSRF (present) | $CO_2$ laser | 10.64 | 500 | 21.7 | $10^9 \sim 10^{10}$ |

## 4. Discussion

Several CBS $\gamma$-ray facilities of 10 MeV order are listed in Table.2. Compared with those facilities, SLEGS has several unique properties.

First of all, SLEGS is expected to achieve flux of non-collimated $\gamma$-ray up to $10^9 \sim 10^{10}$ $s^{-1}$ using a commercial CW $CO_2$ laser of 100W order output power. The high brightness $\gamma$-ray will be a powerful probe to meet requirements of many experimental researches.

Second, since SSRF storage ring has a proper energy to generate $\gamma$-ray of 10MeV order by $CO_2$ laser, SLEGS does not have to use a complicated far infrared (FIR) laser system like BL05SS on SPring-8, so that issues of relatively-low output power, transmission and focusing for operating laser can be avoided.

Last, HI$\gamma$S possesses unique preponderance of the tunable $E_\gamma^{max}$ by using a tunable free electron laser (FEL). However, one of the key issues HI$\gamma$S has to handle is the synchronization between FEL pulses and target electron bunches. While SLEGS will avoid such an issue since the operating laser will run under a CW mode.

To meet the potential requirements of $E_\gamma^{max}$ lower than 22MeV, an oblique injection setup for $CO_2$ laser is within our scope. If the impact angle between laser and electron beam is changeable, one can obtain $\gamma$-ray with determined maximum energy. However, such a setup will definitely cause a decreased $\gamma$-ray flux, thus method like external laser resonator (23) is necessary to enforce power of the operating $CO_2$ laser.

## 5. Summary

In this paper, SLEGS, a $\gamma$-ray beam line based on backward Compton scattering was suggested. SLEGS is expected to achieve a flux of non-collimated $\gamma$-ray up to $10^9 \sim 10^{10}$ $s^{-1}$ by employing a CW mode commercial $CO_2$ laser of 100W order output power. The maximum energy of $\gamma$-ray is about 22MeV.

Acknowledgements

This work was supported by the Knowledge Innovation Program of Chinese Academy of Sciences under Contract No. KJCX2-SW-N13, by the National Natural Science Foundation of China under Contract No. 10475108, No. 10505026, and by the hundred talent project of Shanghai Institute of Applied Physics.

References

[1] R.H. Milburn, Phys. Rev. Lett. 10 (1963) 75
[2] F.R. Arutyunian, V.A. Tumanian, Phys. Lett. 4 (1963) 176
[3] E.L. Saldin, *et al.*, Nucl. Instr. and Meth. A 362 (1995) 574
[4] L. Casano, *et al.*, Laser Unconventional Optics J. 55 (1975) 3
[5] G. Matone, *et al.*, Lect. Notes Phys. 62 (1977) 149
[6] L. Federici, *et al.*, Nuovo Cimento B 59 (1980) 247
[7] D. Babusci, *et al.*, Nucl. Instr. and Meth. A 305 (1991) 19
[8] A. D'Angelo, *et al.*, Nucl. Instr. and Meth. A 455 (2000) 1, and references therein.
[9] S.H. Park, *et al.*, Nucl. Instr. and Meth. A 475 (2001) 425
[10] V.N. Litvinenko, *et al.*, Phys. Rev. Lett. 78 (1997) 4569
[11] H. Ohkuma, *et al.*, Proceedings of EPAC 2006, Edinburgh, Scotland
[12] M. Fujiwara, Prog. Part. and Nucl. Phys. 50 (2003) 487
[13] K. Aoki, *et al.*, Nucl. Instr. and Meth. A 516 (2004) 228

[14] D. Li, *et al.*, Nucl. Instr. and Meth. A 528 (2004) 516
[15] Z.T. Zhao and H.J. Xu, Proceeding of EPAC 2004, Lucerne, Switzerland
[16] W. Greiner and J. Reinhardt, *Quantum Electrondynamics*, Springer-Verlag Berling Heidelberg Press, 1994
[17] Klein O. and Nishina Y., Z. Physik 52 (1929) 853
[18] J. Rossbach and P. Schmüser, *Basic Course on Accelerator Optics*, CERN Yellow Report 94-01.v.1
[19] J. Buon, *Beam Phase Space and Emittance*, CERN Yellow Report 94-01.v.1
[20] Y.M. Jin, *Electron Storage Ring Physics*, University of Science and Technology of China Press, 2001, in Chinese.
[21] C.C. Davis, *Lasers and Electro-Optics*, Cambridge University Press, 1996
[22] G.M. Liu, *et al.*, High Energy Physics and Nuclear Physics 30, Supp-I (2006) 144
[23] I. Will, *et al.*, Nucl. Instr. and Meth. A 472 (2001) 79